Chapter 10

The wind-driven circulation

In Chapter 9 we saw that the ocean comprises a warm, salty, stratified lens of fluid, the thermocline, circulating on top of a cold, fresh, relatively well mixed abyss, as sketched in the schematic, Fig.10.1. The time-mean circulation of thermocline waters is rapid relative to the rather sluggish circulation of the abyss.

There are two processes driving the circulation of the ocean.

1. tangential stresses at the ocean's surface due to the prevailing wind systems which impart momentum to the ocean — the *wind-driven circulation* and

2. convection, induced by loss of buoyancy in polar latitude, due to cooling and/or salt input, causing surface waters to sink to depth, ventilating the abyss — the *thermohaline circulation*.

This separation of the circulation into wind-driven and thermohaline components is somewhat artificial but provides a useful conceptual simplification. In this chapter we will be concerned with the circulation of the warm, salty thermocline waters sketched in Fig.10.1 that are brought in to motion by the wind. We shall see that the effects of the wind blowing over the ocean is to induce, through Ekman pumping or suction (see Section 10.2), a pattern of vertical motion indicated by the arrows on the figure. Pumping down of buoyant surface water in the subtropics and sucking up of heavier interior fluid at the pole and the equator, tilts density surfaces, as sketched in Fig.10.1 and evident in Fig.9.7, setting up a thermal wind shear and geostrophic motion. The presence of jagged topography acts to damp strong mean currents

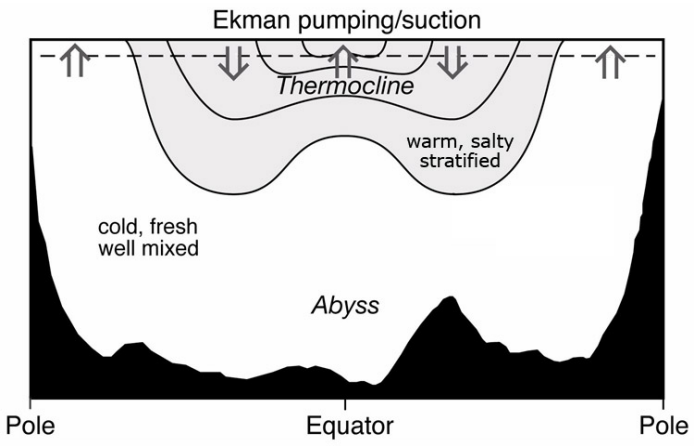

Figure 10.1: The ocean comprises a warm, salty, stratified lens of fluid, the thermocline, circulating on top of a cold, fresh, relatively well mixed, abyss. The surface layer, above the horizontal dotted line at a depth of about 100 m, is driven directly by the wind. The thermocline below is brought in to motion through a pattern of vertical velocity driven by the wind (Ekman pumping and suction) which induces flow in the ocean beneath.

in the abyss. Vertical shears build up across the tilted thermocline, however, supporting strong surface currents. The tilting of the thermocline induced by the collusion of horizontal surface density gradients and vertical motion induced by the wind, leads to a vast store of available potential energy (recall our discussion in Section 8.3.2). We shall see in Section 10.5 that this potential energy is released by baroclinic instability, leading to an energetic eddy field, the ocean's analogue of atmospheric weather systems. Ocean eddies have a horizontal scale of typically 100 km and, as discussed in Chapter 9, are often much stronger than the mean flow, leading to a highly turbulent, chaotic flow — see Fig.9.24. The mean pattern of currents mapped in Figs.9.14 to 9.16 only emerges after averaging over many years.

10.1 The wind stress and Ekman layers

One cannot escape noticing the similarity between the pattern of surface currents in the ocean and that of the low-level winds in the atmosphere. Com-

pare, for example, the pattern of surface elevation of the ocean in Fig.9.19 with the pattern of surface atmospheric pressure, Fig.7.27. Winds, through turbulent transfer of momentum across the atmospheric boundary layer, exert a *stress* on the ocean's surface which drives ocean currents.

The surface wind stress can, to a useful degree of accuracy, be related to the wind velocity through the following relationship (known as a 'bulk formula'):

$$\left(\tau_{wind_x}, \tau_{wind_y}\right) = \rho_{air} c_D u_{10} \left(u_a, v_a\right) \tag{10.1}$$

where $\tau_{wind_x}, \tau_{wind_y}$ are, respectively, the zonal and meridional stress components, c_D is a bulk transfer coefficient for momentum (typically $c_D = 1.5 \times 10^{-3}$), ρ_{air} is the density of air at the surface and u_{10} is the speed of the wind at a height of 10 m. The observed annual average of the stress, computed from Eq.(10.1), is shown in Fig.10.2.

Although there is some similarity between the pattern of surface ocean currents and the pattern of surface wind stress — compare Fig.10.2 with Fig.9.13 — the way in which the ocean responds to this wind stress is fascinating and rather subtle, as we are about to see.

10.1.1 Balance of forces and transport in the Ekman layer

If the Rossby number is small, we can neglect the $\frac{D}{Dt}$ terms in the horizontal momentum Eq.(9.7), reducing them to a three way balance between the Coriolis force, the horizontal pressure gradient and the applied wind-stress forcing. This is just Eq.(7.25) in which $\mathcal{F}$ is interpreted as an applied body force due to the action of the wind on the ocean. First we need to express $\mathcal{F}$ in terms of the wind stress, $\boldsymbol{\tau}_{wind}$.

Consider Fig.10.3 showing a stress which varies with depth, acting on a body of ocean. The stress component of interest here, $\tau_x(z)$, is the $x-$component of force acting at depth z, per unit horizontal area on the layer beneath. Note that the units of τ are $\mathrm{N\,m^{-2}}$. The slab of thickness δz at level z is subjected to a force per unit horizontal area $\tau_x(z+\delta z)$ at its upper surface, but also subjects the layers beneath it to a force $\tau_x(z)$ per unit horizontal area. Therefore the net force per unit horizontal area felt by the layer is $\tau_x(z+\delta z) - \tau_x(z)$. Since the slab has thickness δz, it has volume δz per unit horizontal area, and if the slab has uniform density ρ_{ref}, it has mass $\rho_{ref}\delta z$

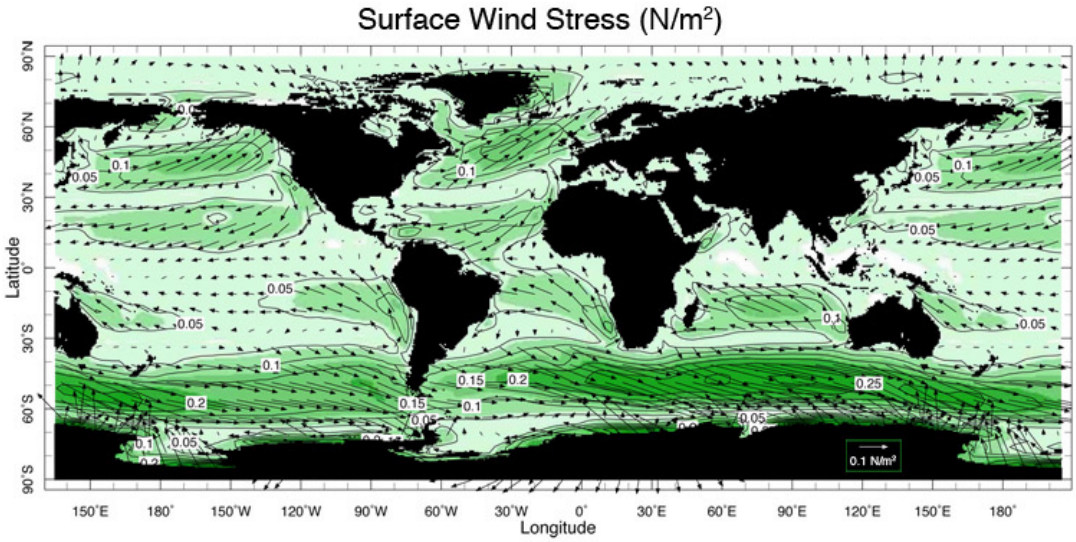

Figure 10.2: Annual mean wind stress on the ocean. A contour of 1 represents a wind-stress of magnitude 0.1 $\mathrm{N\,m^{-2}}$. Stresses reach values of 0.1 to 0.2 $\mathrm{N\,m^{-2}}$ under the middle-latitude westerlies, and are particularly strong in the southern hemisphere. The arrow is a vector of length 0.1 $\mathrm{N\,m^{-2}}$. Note that the stress vectors circulate around the high and low pressure centers shown in Fig.7.27, as one would expect if the surface wind, on which the stress depends, has a strong geostrophic component.

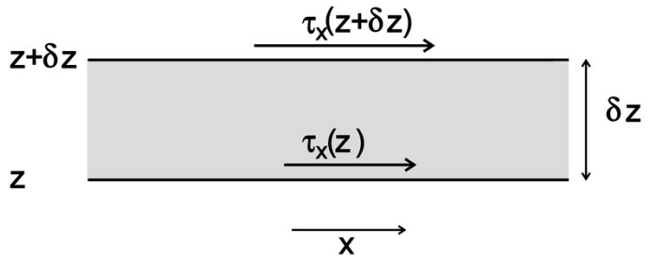

Figure 10.3: The stress applied to an elemental slab of fluid of depth δz is imagined to diminish with depth.

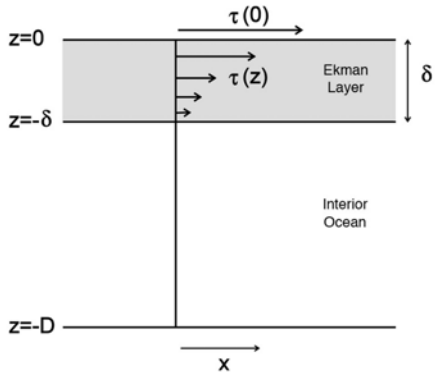

Figure 10.4: The stress at the sea surface, $\tau(0) = \tau_{wind}$, the wind stress, diminishes to zero at a depth $z = -\delta$. The layer directly affected by the stress is known as the Ekman layer.

per unit horizontal area. Therefore the force per unit mass, $\mathcal{F}_x$, felt by the slab is

$$\mathcal{F}_x = \frac{\text{force per unit area}}{\text{mass per unit area}} = \frac{\tau_x(z+\delta z) - \tau_x(z)}{\rho_{ref}\delta z} = \frac{1}{\rho_{ref}}\frac{\partial \tau_x}{\partial z} \ ,$$

for small slab thickness. We can obtain a similar relationship for $\mathcal{F}_y$ and hence write:

$$\mathcal{F} = \frac{1}{\rho_{ref}}\frac{\partial \boldsymbol{\tau}}{\partial z} \tag{10.2}$$

for the horizontal stress vector $\boldsymbol{\tau} = (\tau_x, \tau_y)$. Hence our momentum equation for the steady circulation becomes Eq.(7.25) with $\mathcal{F}$ defined above which, for convenience, we write out in component form here:

$$-fv + \frac{1}{\rho_{ref}}\frac{\partial p}{\partial x} = \frac{1}{\rho_{ref}}\frac{\partial \boldsymbol{\tau}_x}{\partial z} \quad ; \quad fu + \frac{1}{\rho_{ref}}\frac{\partial p}{\partial y} = \frac{1}{\rho_{ref}}\frac{\partial \boldsymbol{\tau}_y}{\partial z} \ . \tag{10.3}$$

Eq.(10.3) describes the balance of forces in the directly wind-driven circulation, but it does not yet tell us what that circulation is. The stress at the surface is known — it is the wind stress, $\boldsymbol{\tau}_{wind}$, plotted in Fig.10.2 —

but we do not know the vertical distribution of stress beneath the surface. The wind stress will be communicated downward by turbulent, wind-stirred motions confined to the near-surface layers of the ocean. The direct influence of wind-forcing decays with depth (rather rapidly — in a few tens of meters or so, depending on wind strength) so that by the time a depth $z = -\delta$ has been reached, the stress has vanished, $\boldsymbol{\tau} = \mathbf{0}$, as sketched in Fig.10.4. As discussed in Chapter 7, this is the 'Ekman layer'.

Conveniently, we can bypass the need to know the detailed vertical distribution of $\boldsymbol{\tau}$ by focusing on the transport properties of the layer by integrating vertically across it. As in Section 7.4, we split the flow into geostrophic and ageostrophic parts. With $\mathcal{F}$ given by Eq.(10.2), the ageostrophic component of Eq.(7.25) is

$$f\widehat{\mathbf{z}} \times \mathbf{u}_{ag} = \frac{1}{\rho_{ref}} \frac{\partial \boldsymbol{\tau}}{\partial z} \, . \tag{10.4}$$

Multiplying Eq.(10.4) by ρ_{ref} and integrating across the layer from the surface where $\boldsymbol{\tau} = \boldsymbol{\tau}_{wind}$, to a depth $z = -\delta$, where $\boldsymbol{\tau} = 0$ — see Fig.10.4 — we obtain:

$$f\widehat{\mathbf{z}} \times \mathbf{M}_{Ek} = \boldsymbol{\tau}(z = 0) = \boldsymbol{\tau}_{wind}$$

where

$$\mathbf{M}_{Ek} = \int_{-\delta}^{0} \rho_{ref} \mathbf{u}_{ag} dz$$

is the lateral mass transport over the layer. Noting that $\widehat{\mathbf{z}} \times (\widehat{\mathbf{z}} \times \mathbf{M}_{Ek}) = -\mathbf{M}_{Ek}$ we may rearrange the above to give:

$$\mathbf{M}_{Ek} = \frac{\boldsymbol{\tau}_{wind} \times \widehat{\mathbf{z}}}{f}. \tag{10.5}$$

Since $\widehat{\mathbf{z}}$ is a unit vector pointing vertically upwards, we see that the mass transport of the Ekman layer is exactly to the right of the surface wind (in the northern hemisphere). Eq.(10.5) determines $\mathbf{M}_{Ek}$, which depends *only* on $\boldsymbol{\tau}_{wind}$ and f. But Eq.(10.5) does not predict typical velocities or boundary layer depths which depend on the details of the turbulent boundary layer.

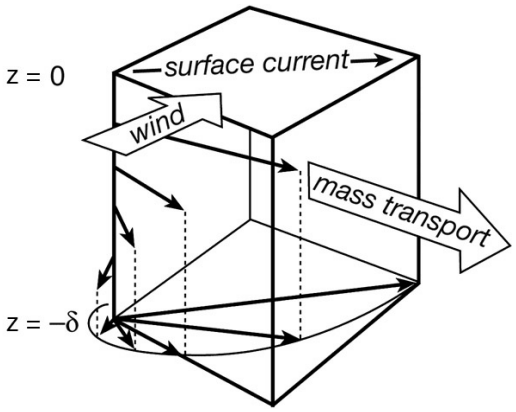

Figure 10.5: The mass transport of the Ekman layer is directed to the right of the wind in the Northern Hemisphere — see Eq.(10.5). Theory suggests that horizontal currrents, u_{ag}, within the Ekman layer spiral with depth as shown.

A more complete analysis (carried out by Ekman, 1905[1]) shows that the horizontal velocity vectors within the layer trace out a spiral, as shown in Fig.10.5. Typically $\delta \simeq 10 - 100\,\mathrm{m}$. So the direct effects of the wind are confined to the very surface of the ocean.

[1] Vagn Walfrid Ekman (1874-1954) a Swedish physical oceanographer, is remembered for his studies of wind-driven ocean currents. The role of Coriolis forces in the wind-driven layers of the ocean was first suggested by the great Norwegian explorer Fridtjof Nansen who observed that sea ice generally drifted to the right of the wind and proposed that this was a consequence of the Coriolis force. He suggested the problem to Ekman — at the time a student of Vilhelm Bjerknes — who, remarkably, worked out the mathematics behind what are now known as Ekman spirals, in one evening of intense activity.

10.1.2 Ekman pumping and suction and GFD Lab XII

Imagine a wind-stress blowing over the northern hemisphere ocean with the general anticyclonic pattern sketched in Fig.10.6(left). We have just seen that the Ekman transport is directed to the right of the wind and hence there will be a mass flux directed inwards (as marked by the broad open arrows in the figure), leading to convergence in to the center. Since the mass flux across the sea surface is zero (neglecting evaporation and precipitation which, as discussed in Chapter 11, are typically $\pm 1\,\mathrm{m\,y^{-1}}$), water cannot accumulate in the steady state and so it must be driven down into the interior. Conversely, the cyclonic pattern of wind-stress sketched in Fig.10.6(right) will result in a mass flux directed outwards from the center and therefore water will be drawn up from below.

If the wind-stress pattern varies in space (or, more precisely, as we shall see, if the wind-stress has some 'curl') it will therefore result in vertical motion across the base of the Ekman layer. The flow within the Ekman layer is convergent in *anticyclonic* flow and divergent in *cyclonic* flow, as sketched in Fig.10.6. The convergent flow drives downward vertical motion (called Ekman pumping); the divergent flow drives upward vertical motion from beneath (called Ekman suction). We will see that it is this pattern of vertical motion from the base of surface Ekman layers that brings the interior of the ocean in to motion. But first let us study Ekman pumping and suction in isolation, in a simple laboratory experiment.

GFD Lab XII: Ekman pumping and suction

The mechanism by which the wind drives ocean circulation through the action of Ekman layers can be studied in a simple laboratory experiment in which the cyclonic and anticyclonic stress patterns sketched in Fig.10.6 are created by driving a disc around on the surface of a rotating tank of water — see Fig.10.7 and legend. We apply a stress by rotating a disc at the surface of a tank of water which is itself rotating, as depicted in Fig.10.7. If $\Omega > 0$, the stress imparted to the fluid below by the rotating disc will induce an ageostrophic flow to the right of the stress (Eq.(10.5)): outward if the disc is rotating cyclonically relative to the rotating table $\left(\frac{\omega}{\Omega} > 0\right)$, inward if the disc is rotating anticyclonically $\left(\frac{\omega}{\Omega} < 0\right)$, as illustrated in Fig.10.6. The Ekman layers and patterns of upwelling and downwelling can be made visible through the use of dye crystals.

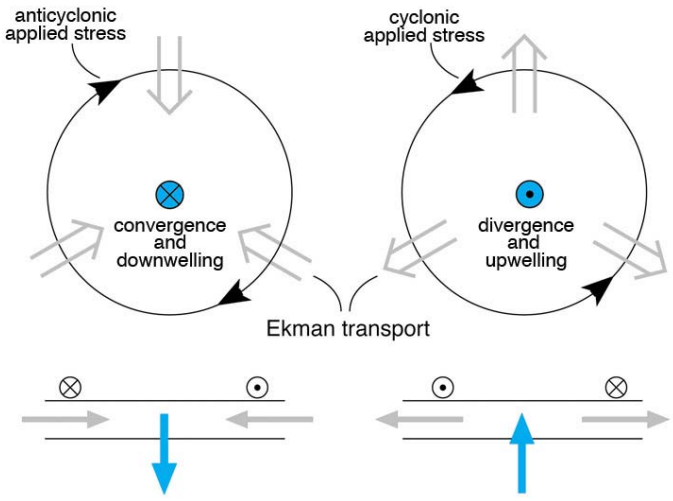

Figure 10.6: The Ekman transport is directed prependicular to the applied stress (to the right if $\Omega > 0$, to the left if $\Omega < 0$) driving (left) convergent flow if the stress is anticyclonic and (right) divergent flow if the stress is cyclonic. (The case $\Omega > 0$ — the northern hemisphere — is shown.)

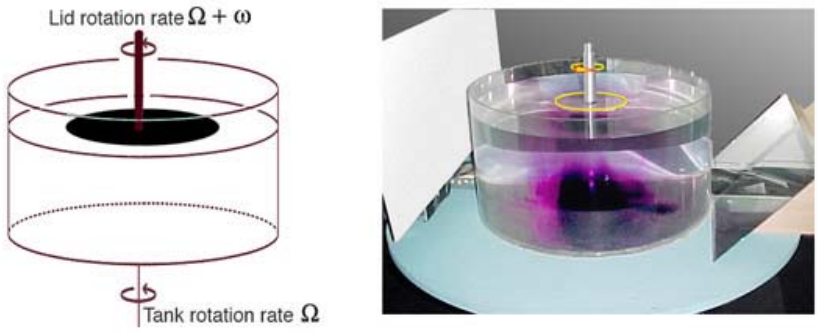

Figure 10.7: We rotate a disc at rate ω on the surface of a cylindrical tank of water (in fact the disc is just submerged beneath the surface). The tank of water and the disc driving it are then rotated at rate Ω using a turntable: 10 rpm works well. We experiment with disc rotations of both signs, $\omega = \pm 5$ rpm. Low values of $|\omega|$ are used to minimize the generation of shearing instabilities at the edge of the disc. The apparatus is left for about 20 minutes to come to equilibrium. Once equilibrium is reached, dye crystals are dropped in to the water to trace the motions. The whole system is viewed from above in the rotating frame; a mirror can be used to capture a side view, as shown in the photograph on the right.

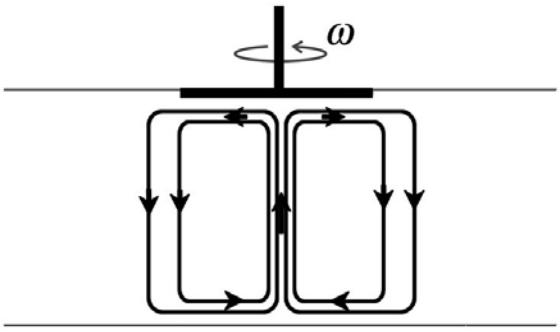

Figure 10.8: Schematic of the ageostrophic flow driven by the cyclonic rotation of a surface disc relative to a homogeneous fluid that is itself rotating cyclonically below. Note that the flow in the bottom Ekman layer is in the same sense as Fig.7.23, top panel, from GFDLab X. The flow in the top Ekman layer is divergent. If the disc is rotated anticyclonically, the sense of circulation is reversed.

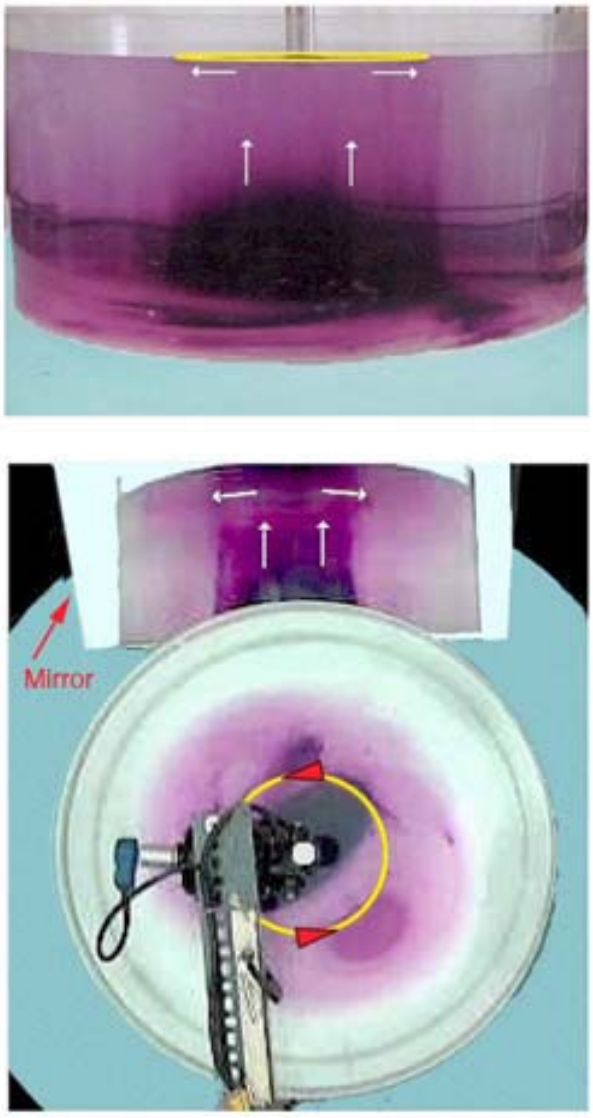

Figure 10.9: (Top) The anticlockwise rotation of the disc at the surface induces upwelling in the fluid beneath (Ekman suction) as can be clearly seen from the 'dome' of dyed fluid being drawn up from below. (Bottom) We see the experiment from the top and, via the mirror, from the side (and slightly below). Now, sometime later, the dye has been drawn up in to a column reaching right up to the disk and is being expelled outward at the top. The white arrows indicate the general direction of flow. The yellow line marks the rotating disk.

With Ω, $\omega > 0$ (i.e. disk rotating cyclonically and faster than the table) the column of fluid is brought into cyclonic circulation and rubs against the bottom of the tank. The flow in the bottom Ekman layer is then just as it was for the cyclonic vortex studied in GFD Lab X (Fig.7.23, top panel) and is directed inwards at the bottom as sketched in Fig.10.8. Convergence in the bottom Ekman layer thus induces upwelling, drawing fluid up toward the rotating disc at the top, where it diverges in the Ekman layer just under the disk). This is clearly evident in the photographs of upwelling fluid shown in Fig.10.9. The Ekman layer directly under the disc drives fluid outwards to the periphery, drawing fluid up from below. This process is known as 'Ekman suction'.

If the disc is rotated anticyclonically, convergence of fluid in the Ekman layer underneath the disc drives fluid downward into the interior of the fluid in a process known as 'Ekman pumping' (in this case the sign of all the arrows in Fig.10.8 is reversed).

Before going on to discuss how Ekman pumping and suction manifest themselves on the large scale in the ocean, it should be noted that in this experiment the Ekman layers are laminar (non-turbulent) and controlled by the viscosity of water.[2] In the ocean the momentum of the wind is carried down in to the interior by turbulent motions rather than by molecular processes. Nevertheless, the key result of Ekman theory, Eq.(10.5), still applies. We now go on to estimate typical Ekman pumping rates in the ocean.

10.1.3 Ekman pumping and suction induced by large-scale wind patterns

Fig.10.10 shows a schematic of the midlatitude westerlies (eastward wind stress) and the tropical easterlies (westward stress) blowing over the ocean, as suggested by Fig.10.2. Because the Ekman transport is 'to the right of the wind' in the northern hemisphere, there is convergence and downward

[2] Theory tells us (not derived here, but see Hide and Titman; 1967) that:

$$w_{Ek} = \frac{\omega}{2}\left(\frac{\nu}{2\Omega+\omega}\right)^{\frac{1}{2}}$$

where $\nu = 10^{-6}\,\mathrm{m^2\,s^{-1}}$ is the kinematic viscosity of water (see Table 9.3). In the experiment of Fig.10.7 typically $\Omega = 1\,\mathrm{rad\,s^{-1}}$ (that is 10 rpm) and $\omega = 0.5\,\mathrm{rad\,s^{-1}}$, and so $w_{Ek} \simeq 1.5\times10^{-4}\,\mathrm{m\,s^{-1}}$. Thus in Fig.10.9, fluid is sucked up at a rate of order 9 cm every 10 minutes or so.

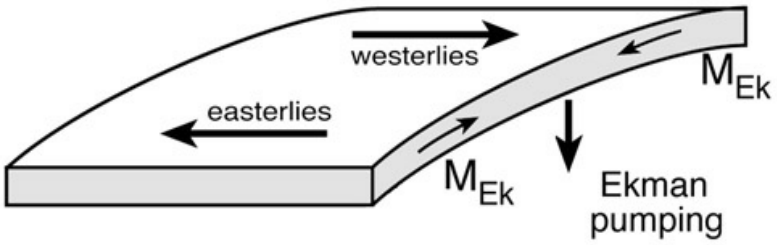

Figure 10.10: A schematic showing midlatitude westerlies (eastward wind stress) and tropical easterlies (westward stress) blowing over the ocean. Because the Ekman transport is 'to the right of the wind' in the northern hemisphere, there is convergence and downward Ekman pumping in to the interior of the ocean. Note that the sea surface is high in regions of convergence.

Ekman pumping in the subtropics. This Ekman layer convergence also explains why the sea-surface is higher in the subtropics than in subpolar regions (cf. Fig.9.19): the water is 'piled up' by the wind through the action of counter-posed Ekman layers, as sketched in Fig.10.10. So the interior of the subtropical ocean 'feels' the wind stress indirectly, through Ekman-induced downwelling. It is this downwelling that, for example, causes the $\sigma = 26.5$ surface plotted in Fig.9.8 to bow down in the subtropics. Over the subpolar oceans, by contrast, where the westward stress acting on the ocean diminishes in strength moving northwards (see Fig.10.2), Ekman suction is induced, drawing fluid from the interior upward into the Ekman layer (as in GFD Lab XII, just described). Hence isopycnals are drawn up to the surface around latitudes of 60°N, S. This general pattern of Ekman pumping/suction imposed on the interior ocean is represented by the vertical arrows in the schematic Fig.10.1.

We can obtain a simple expression for the pattern and magnitude of the Ekman pumping/suction field in terms of the applied wind-stress as follows. Integrating the continuity equation, Eq.(6.11), across the Ekman layer, assuming that geostrophic flow is non-divergent (but see footnote in Section 10.2.1):

$$\nabla_h \cdot \mathbf{u}_{ag} + \frac{\partial w}{\partial z} = 0, \tag{10.6}$$

and noting $w = 0$ at the sea surface, then the divergence of the Ekman layer transport results in a vertical velocity at the bottom of the Ekman layer which has magnitude, using Eq.(10.5):

$$w_{Ek} = \frac{1}{\rho_{ref}} \nabla_h \cdot \mathbf{M}_{Ek} \tag{10.7}$$

$$= \frac{1}{\rho_{ref}} \widehat{\mathbf{z}} \cdot \nabla \times \left(\frac{\boldsymbol{\tau}_{wind}}{f} \right) = \frac{1}{\rho_{ref}} \left(\frac{\partial}{\partial x} \frac{\tau_{wind_y}}{f} - \frac{\partial}{\partial y} \frac{\tau_{wind_x}}{f} \right) \tag{10.8}$$

(see Appendix 13.2.2, III). The Ekman pumping velocity defined in Eq.(10.7) depends on the curl of $\left(\frac{\boldsymbol{\tau}_{wind}}{f} \right)$. Note, however, that typically $\boldsymbol{\tau}_{wind}$ varies much more than f and so the pattern of w_{Ek} is largely set by variations in $\boldsymbol{\tau}_{wind}$. We can estimate the magnitude of w_{Ek} as follows. Fig.10.2 shows that $\boldsymbol{\tau}_{wind}$ changes from $+ \, 0.1 \, \mathrm{N \, m^{-2}}$ to $- \, 0.1 \, \mathrm{N \, m^{-2}}$ over 20° of latitude, or 2000 km. Thus, Eq.(10.7) suggests: $w_{Ek} \approx \frac{1}{10^3 \, \mathrm{kg \, m^{-3}}} \times \frac{0.2 \, \mathrm{N \, m^{-2}}}{10^{-4} \, \mathrm{s^{-1}} \times 2 \times 10^6 \, \mathrm{m}} = 32 \, \mathrm{m \, y^{-1}}$. It is interesting to compare this with the annual-mean precipitation rate over the globe of about $1 \, \mathrm{m \, y^{-1}}$ (this quantity is plotted in Fig.11.6). We see that the wind, through the action of Ekman layers, achieves a vertical volume flux which is some $30 - 50$ times larger than a typical annual-mean precipitation rate!

Fig.10.11 shows the global pattern of w_{Ek} computed from the surface stress distribution shown in Fig.10.2, using Eq.(10.7). First of all, note the white band along the equator where the calculation was not attempted because $f \longrightarrow 0$ there. In fact, however, the equatorial strip is a region of upwelling because the trade winds on either side of the equator drive fluid away from the equator in the surface Ekman layer, and so demand a supply of fluid from below (as will be seen in Section 12.2). Away from the equator we observe downwelling in the subtropics and upwelling in subpolar regions with typical magnitudes of $50 \, \mathrm{m \, y^{-1}}$, pushing down and pulling up the isopycnals in Fig.9.7. It takes about 8 y to pump water down from the surface to 400 m, a typical thermocline depth (cf. Fig.9.8) indicative of the timescale operating in the thermocline. Note that the zero Ekman pumping contours in Fig.10.11 separate the ocean into geographical domains which will be central to our understanding of the pattern of ocean gyres seen in Figs.9.14 — 9.16 and large-scale property distributions[3]. It is these broad domains, demarcated

[3]The pattern of Ekman pumping imposed on the ocean by the wind, Fig.10.11, has a profound influence on the distribution of dynamically important tracers (such as T, S) the

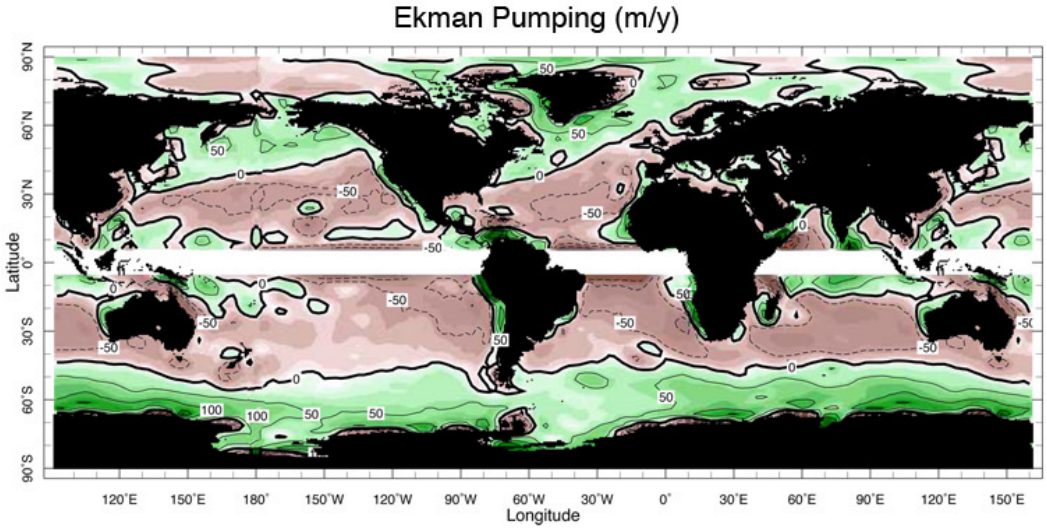

Figure 10.11: The global pattern of Ekman vertical velocity ($\mathrm{m\,y^{-1}}$) computed using Eq.(10.7) from the annual mean wind-stress pattern shown in Fig.10.2. Motion is upward in the green areas, downward in the brown areas. w_{Ek} is not computed over the white strip along the equator because $f \longrightarrow 0$ there. The thick line is the zero contour. Computed from Trenberth et al (1989) data. The broad regions of upwelling and downwelling delineated here are used to separate the ocean in to different dynamical regimes, as indicated by the colors in Fig.9.13.

by zero wind-stress curl lines, that are color-coded in Fig.9.13: subpolar regions (blue) are generally subjected to upwelling, subtropical regions (yellow) to downwelling and tropical regions (red) to upwelling.

What, then, is the response of the interior ocean to this pattern of upwelling and downwelling imposed from above?

---

focus of attention here, but also on biologically important properties such as nutrients. Subpolar gyres, for example, are replete in nutrients because of upwelling of nutrient-rich waters from below and so are regions of high biological productivity. Conversely, subtropical gyres are relative deserts, biologically-speaking, because downwelling driven by the wind pushes the nutrients away from the sunlit upper layer where photosynthesis can take place. Thus Ekman pumping has both physical and biogeochemical consequences for the ocean.

10.2 Response of the interior ocean to Ekman pumping

10.2.1 Interior balances

Beneath the Ekman layer the flow is in geostrophic balance. How does this geostrophic flow respond to the imposed pattern of vertical velocity from the Ekman layer shown in Fig.10.11? To study the effect of w on the interior ocean we make use of the continuity equation, Eq.(6.11), applied to the interior flow, assumed to be geostrophic. Taking the horizontal divergence of the geostrophic flow we find:

$$\nabla_h \cdot \mathbf{u}_g = \frac{\partial}{\partial x}\left(-\frac{1}{\rho_{ref}\ f}\frac{\partial p}{\partial y}\right) + \frac{\partial}{\partial y}\left(\frac{1}{\rho_{ref}\ f}\frac{\partial p}{\partial x}\right) = -\frac{\beta}{f}v_g \tag{10.9}$$

where we have remembered that f varies with y and, noting that $dy = ad\varphi$,

$$\beta = \frac{df}{dy} = \frac{1}{a}\frac{df}{d\varphi} = \frac{2\Omega}{a}\cos\varphi \tag{10.10}$$

is the meridional gradient in the Coriolis parameter, Eq.(6.42). The variation of f with latitude is known as the '$\beta-$effect'.

We see, then, that because f varies with latitude the geostrophic flow is horizontally divergent. Hitherto (in Eq.(10.6), for example) we have assumed that $\nabla_h \cdot \mathbf{u}_g = 0$. However, on the planetary scales being considered here, we can no longer ignore variations in f and the resulting horizontal divergence of geostrophic flow is associated with vertical stretching of water columns because[4]:

$$\nabla_h \cdot \mathbf{u}_g + \frac{\partial w}{\partial z} = 0. \tag{10.11}$$

Combining Eqs.(10.9 and 10.11) we obtain the very useful expression :

$$\beta v_g = f\frac{\partial w}{\partial z} \tag{10.12}$$

[4]Eq.(10.11) tells us that $\nabla_h \cdot \mathbf{u}_g \sim \frac{w_{Ek}}{H}$ where H is the vertical scale of the thermocline, and so is $\frac{\delta}{H}$ smaller than $\nabla_h \cdot \mathbf{u}_{ag} = \frac{w_{Ek}}{\delta}$ in Eq.(10.6) where δ is the Ekman layer depth. Because $\frac{\delta}{H} \lesssim 0.1$, we are thus justified in neglecting $\nabla_h \cdot \mathbf{u}_g$ in comparison with $\nabla_h \cdot \mathbf{u}_{ag}$ in the computation of w_{Ek}, as was assumed in deriving Eq.(10.7).

which relates horizontal and vertical currents.

If vertical velocities in the abyss are much smaller than surface Ekman pumping velocities, then Eq.(10.12) tells us that ocean currents will have a southward component in regions where $w_{Ek} < 0$ and northward where $w_{Ek} > 0$. This is indeed observed in the interior regions of ocean gyres: consider Figs.9.14 and 9.15, for example, in the light of Eq.(10.12) and Fig.10.11. Does Eq.(10.12) make any quantitative sense? Putting in numbers: $f = 10^{-4}\,\mathrm{s}^{-1}$, $w_{Ek} = 30$ m y^{-1}, H the depth of the thermocline $\sim 1\,$km, we find that $v = 1$ cm s^{-1}, typical of the gentle currents observed in the interior of the ocean on the large-scales (note that Fig.9.22top shows *surface* currents, whereas our estimate here is an average current over the depth of the thermocline). This is the basic mechanical drive of the ocean circulation: the pattern of Ekman pumping imposed on the ocean from above induces meridional motion through Eq.(10.12).

10.2.2 Wind-driven gyres and western boundary currents

We have seen that Ekman pumping, downward in to the interior of the ocean, must drive an equatorward flow in the subtropical latitude belt between the midlatitude westerlies and tropical easterlies. Although this flow is indeed observed (see the equatorward interior flow over the subtropics in Figs.9.14 and 9.15), we have not yet explained the remainder of the circulation. If we take a very simple view of the geometry of the midlatitude ocean basins (Fig.10.12), then the equatorward flow induced by Ekman pumping could be "fed" at its poleward side by eastward or westward flow, and in turn feed westward or eastward flow at the equatorward edge; either would be consistent with Eq.(10.12), which only dictates the N-S component of the current. However, the general sense of circulation must mirror the anticyclonic sense of the driving wind stress in Fig.10.12. Hence the required poleward return flow must occur on the western margin, as sketched in Fig.(10.12).[5] In the resulting intense *western boundary current*, our assumptions of geostrophy

[5]Indeed, to sustain the circulation against frictional dissipation at the bottom and side boundaries, the wind stress must *do work* on the ocean. Since the rate of doing work is proportional to the product of wind stress and current velocity ($\mathbf{u} \cdot \mathcal{F} > 0$) these two quantities must, on average, be in phase in order for the work done to be positive. This is the case if the sense of circulation is as depicted in Fig.10.12, whereas the work done would be negative if the circulation were returned to the east.

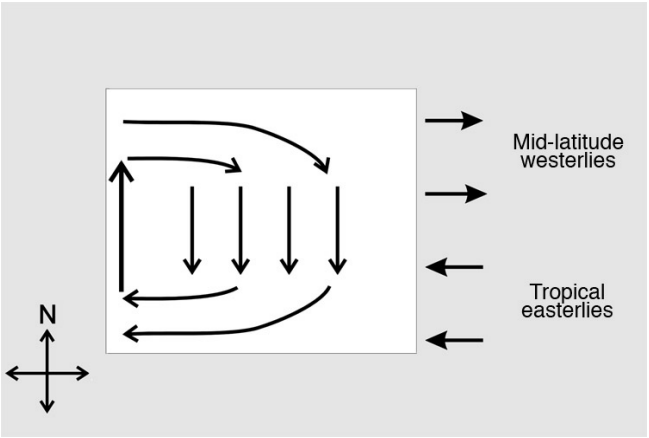

Figure 10.12: Schematic diagram showing the sense of the wind-driven circulation in the interior and western boundary regions of subtropical gyres.

and/or of negligible friction break down (as will be discussed in more detail in Section 11.3.3) and therefore Eq.(10.12) is not applicable. This current is the counterpart in our simple model of the Gulf Stream or the Kuroshio, and other western boundary currents.

The preference for western as opposed to eastern boundary currents is strikingly evident in the surface drifter observations shown in Fig.10.13, which displays the same data as in Fig.9.15 but zooms in at high resolution on the surface circulation in the North Atlantic. We clearly observe the northward flowing Gulf Stream and the southward flowing Labrador Current hugging the western boundary. Here mean currents can exceed $40\,\mathrm{cm\,s^{-1}}$. Note how the path of the Gulf Stream and its interior extension, the North Atlantic Current, tends to follow the zero Ekman pumping line in Fig.10.11, which marks the boundary between the subtropical and subpolar gyres and the region of enhanced temperature gradients.

10.2.3 Taylor-Proudman on the sphere

Before going on in Section 10.3 to a fuller discussion of the implications of Eq.(10.12) on ocean circulation, we now discuss what it means physically. Eq.(10.12) can be simply understood in terms of the attendant rotational and geometrical constraints on the fluid motion, i.e. the Taylor-Proudman

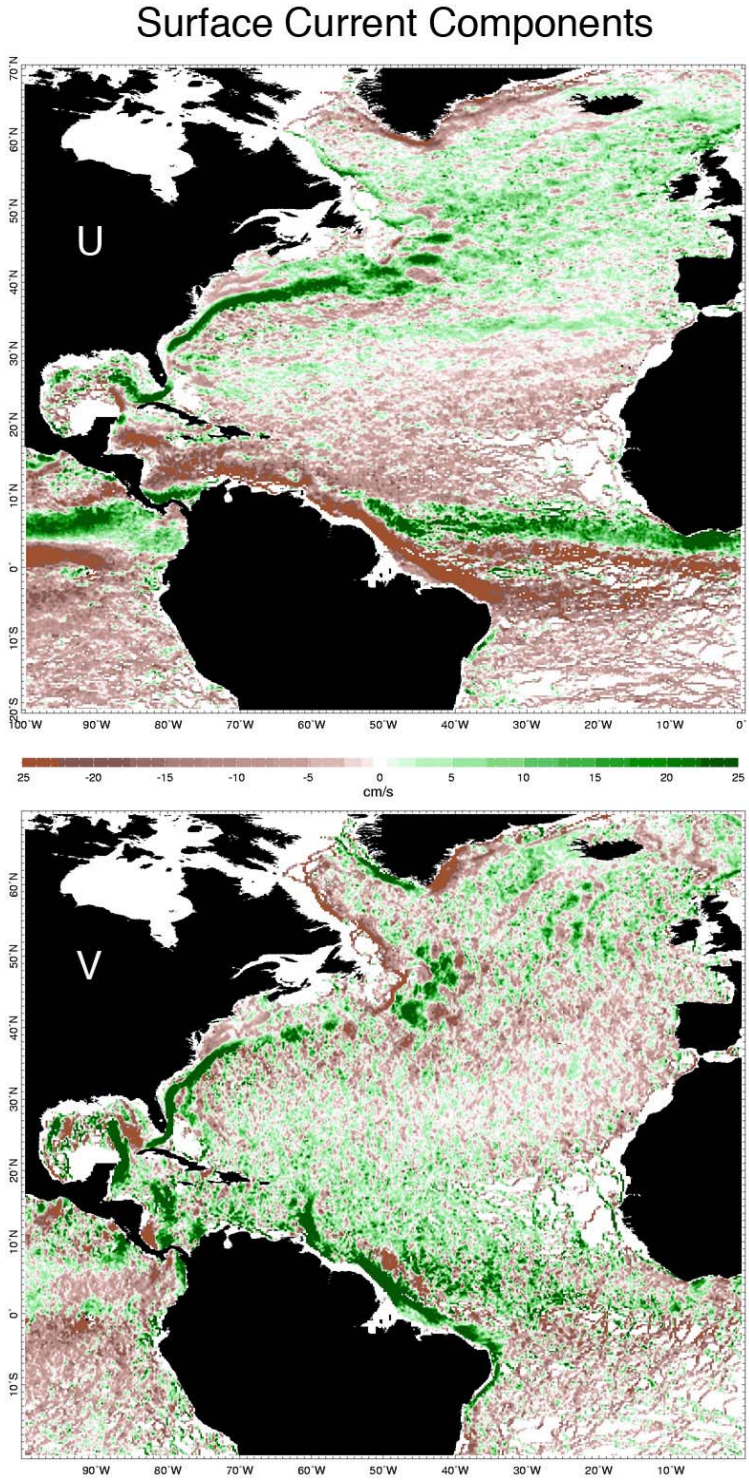

Figure 10.13: (Top) Time-mean zonal velocity and (Bottom) the meridional velocity in $\mathrm{cm\,s^{-1}}$ computed from surface drifters averaged over a $0.25^\circ \times 0.25^\circ$ grid over the North Atlantic (Data courtesy of Maximenko and Niiler, 2003).

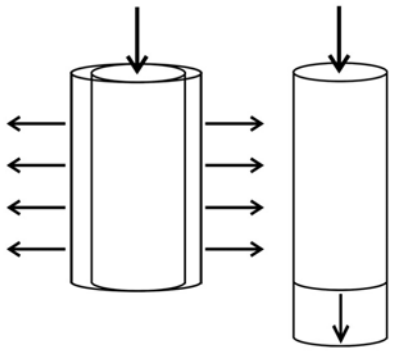

Figure 10.14: In Section 10.2.3 we consider the possibility that a Taylor column subjected to Ekman pumping at its top might conserve mass by expanding its girth, as sketched on the left. We argue that such a scenario is not physically plausible. Instead the column maintains its cross-sectional area and increases its length, as sketched on the right.

theorem on the sphere. This can be seen as follows.

Let us first consider rotational constraints on the possible motion. If the ocean were homogeneous then, as described in Section 7.2, the steady, inviscid, low-Rossby-number flow of such a fluid must obey the Taylor-Proudman theorem, Eq.(7.14). Thus, the velocity vector cannot vary in the direction parallel to the rotation vector and flow must be organized into columns parallel to $\mathbf{\Omega}$, an expression of gyroscopic rigidity, as illustrated in GFD Lab VII, Section 7.2.1 and sketched in Fig.7.8.

Now, consider what happens to such a column of fluid subjected to Ekman pumping at its top. According to Eq.(7.14), we might think that mass continuity would be satisfied by uniform flow sideways out of the column, as sketched in Fig.10.14.

This satisfies the constraint that the flow be independent of height, but cannot be sustained in a steady flow. Why not? If the flow is axisymmetric about the circular column, it will conserve its angular momentum, $\Omega r^2 + v_\theta r$, where v_θ is the azimuthal component of flow around the column, and r is the column radius. The column must continuously expand as fluid is being pumped into it at its top; thus r must increase and so v_θ must change by an amount $\delta v_\theta \simeq -2\Omega\delta r$ (this, of course, is just Eq.(7.22)) as the column increases its girth by an amount δr. Thus v_θ must become increasingly neg-

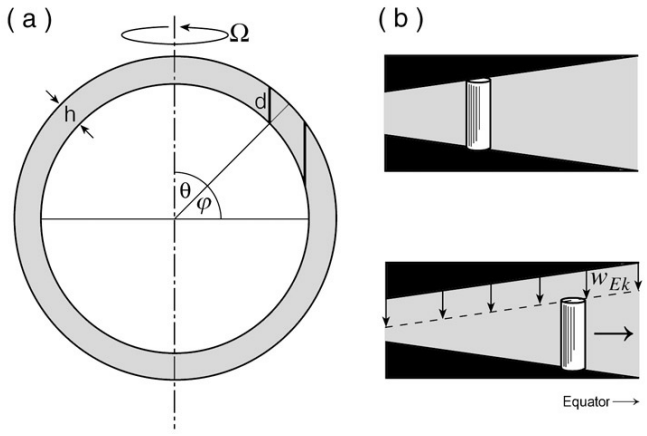

Figure 10.15: (a) An illustration of Taylor-Proudman on a rotating sphere. We consider a spherical shell of homogeneous fluid of constant thickness h. Taylor columns line up parallel to Ω with length d. The latitude is φ and the colatitude θ. (b) A Taylor column in a wedge. If the wedge narrows, or fluid is pumped down from the top at rate w_{Ek}, the Taylor column moves sideways to the thicker end of the wedge. This is just how one flicks a lemon seed. The downward motion between finger and thumb generates lateral (shooting) motion as the seed slips sideways. Modified from a discussion by Rhines (1993).

ative as r increases. This is obviously inconsistent with our assumption of steady state and not physically reasonable.

So, what else can happen? Let's now introduce the geometrical constraint that our Taylor columns must move in a spherical shell, as sketched in Fig.10.15a. (We have obviously exaggerated the depth h of the fluid layer in the figure — recall Fig.1.1!) We see that the columns have greatest length, in the direction parallel to Ω, near the equator. Therefore, if supplied by fluid from above by systematic Ekman pumping, a fluid column can expand in volume without expanding its girth (which we have seen is not allowed in steady state), by *moving systematically equatorward* in the spherical shell and hence increasing its length in the manner illustrated in Fig.10.15b. The column will move equatorward at just the rate required to ensure that the 'gap' created between it and the spherical shell is at all times filled by the pumping down of water from the surface; this, in essence, is how the wind, through the Ekman layers, drives the circulation in the interior of the ocean. The rate

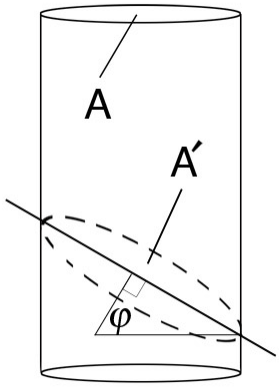

Figure 10.16: The area $A' = \frac{A}{\sin\varphi}$ is the cross-sectional area of a Taylor column, A, projected on to the surface of the sphere, where φ is the latitude.

at which fluid is pumped down from the Ekman layer must be equal to the rate of change of the volume of the Taylor columns beneath.

Let's think about this process in more detail following Fig.10.15. The Taylor columns are aligned parallel to the rotation axis; hence, since $\cos\theta = \sin\varphi = \frac{h}{d}$ where θ is colatitude and φ latitude (see Fig.10.15a), their length is given by:

$$d = \frac{h}{\sin\varphi} \tag{10.13}$$

if the shell is thin (this is inaccurate within less than 1% of the equator). If the change in the volume of the Taylor column is $A\frac{Dd}{Dt}$, where (see Fig.10.16) A is its cross-sectional area measured perpendicular to Ω (which, as discussed above, does not change in time) and d is its length parallel to Ω then

$$A' w_{Ek} = \frac{A}{\sin\varphi} w_{Ek} = \frac{A}{\sin\varphi}\left(-\frac{Dh}{Dt}\right) = -A\frac{Dd}{Dt}$$

since $A' = \frac{A}{\sin\varphi}$ is the area of the Taylor column projected on to the surface of the sphere over which fluid is being pumped down from the Ekman layer at rate w_{Ek}. Note that the minus sign ensures that if $w_{Ek} < 0$ (pumping down in to the ocean), then $\frac{Dd}{Dt} > 0$: i.e., *following the Taylor Column along* its length increases.

Rewriting,

$$\frac{w_{Ek}}{\sin\varphi} = -\frac{Dd}{Dt} = -\frac{D\varphi}{Dt}\frac{dd}{d\varphi} = \frac{D\varphi}{Dt}\left(\frac{h\cos\varphi}{\sin^2\varphi}\right) = \frac{v}{a}\left(\frac{h\cos\varphi}{\sin^2\varphi}\right) \qquad (10.14)$$

where Eq.(10.13) has been used and $v = a\frac{D\varphi}{Dt}$ is the meridional velocity of the column. Multiplying both sides by 2Ω and rearranging, Eq.(10.14) may be written in the form:

$$\beta v = f\frac{w_{Ek}}{h} \qquad (10.15)$$

where f is given by Eq.(6.42) and β by Eq.(10.10). Note that, setting $\frac{\partial w}{\partial z} = \frac{w_{Ek}}{h}$, we have arrived at a version of Eq.(10.12).

The simple mechanism sketched in Fig.10.15b is the basic drive of the wind-driven circulation; the gentle vertical motion induced by the prevailing winds, w_{Ek}, is amplified by a large geometrical factor, $\frac{f}{\beta h} = \frac{a}{h}\tan\varphi \simeq \frac{\text{radius of Earth}}{\text{depth of ocean}} \sim 1000$, to create horizontal currents with speeds that are 1000 times that of Ekman pumping rates, i.e., $1\,\mathrm{cm\,s^{-1}}$ compared to $30\,\mathrm{m\,y^{-1}}$. Thus we see that the stiffness imparted to the fluid by rotation results in strong lateral motion as the Taylor Columns are squashed and stretched in the spherical shell.

There are two useful mechanical analogies:

1. 'pip' flicking: a lemon seed shoots out sideways on being squashed between finger and thumb — see Fig.10.15b.

2. a child's spinning top: the 'pitch' of the thread on the spin axis results in horizontal motion when the axis is pushed down — see Fig.10.17. The tighter the pitch the more horizontal motion one creates (note, however, that in practice friction prevents use of a very tight pitch).

10.2.4 GFD Lab XIII: Wind-driven ocean gyres

The above discussion motivates a laboratory demonstration of the wind-driven circulation. We need the following three essential ingredients: (i) geometrical and (ii) rotational constraints and (iii) a representation of Ekman pumping. The apparatus, shown in Fig.10.18, consists of a rotating Plexiglas disc (to represent the action of the wind as in GFD Lab XII) on the surface of a anticlockwise-rotating square tank of water with a sloping bottom (to

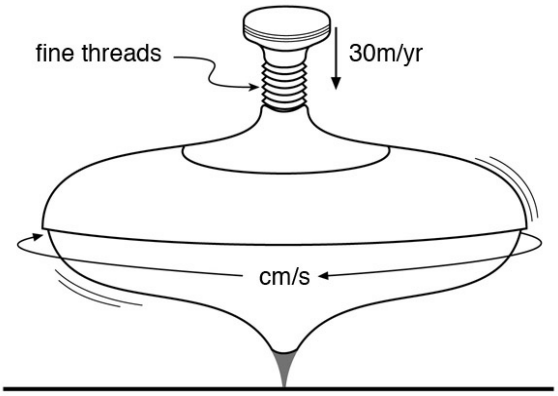

Figure 10.17: The mechanism of wind-driven ocean circulation can be likened to that of a child's spinning top. The tight pitch of the screw thread (analogous to rotational rigidity) translates weak vertical motion (Ekman pumping of order 30 $\mathrm{m\,y^{-1}}$) in to rapid horizontal swirling motion (ocean gyres circulating at speeds of cm $\mathrm{s^{-1}}$).

represent, as we shall see, spherical geometry). The stress applied by the rotating lid to the underlying water is analogous to the wind stress at the ocean surface. With clockwise differential rotation of the disc (Fig.10.6, left), fluid is drawn inwards in the Ekman layer just under the lid and pumped downwards in to the interior, mimicking the pumping down of water in subtropical gyres by the action of the winds, as sketched in Fig.10.10. The varying depth of the tank mimics the variation in the depth of the spherical shell measured in the direction parallel to the rotation vector on the sphere (Fig.10.15). The shallow end of the tank is thus analogous to the poleward flank of the ocean basin (the 'N' in Figs.10.18 and 10.19) and the deep end to the tropics.

On introduction of dye (through bore holes in the Plexiglas disc) to help visualize the flow we observe a clockwise (anticyclonic) gyre with interior flow moving towards the deep end of the tank ('equatorward') as charted in Fig.10.19. This flow (except near the lid and the bottom) will be independent of depth because the interior flow obeys the Taylor-Proudman theorem. Consistent with the discussion see Section 10.2.2, a strong "poleward" return flow forms at the "western" boundary; this is the tank's equivalent of the Gulf Stream in the Atlantic or the Kuroshio in the Pacific.

In a manner directly analogous to that described in Section 10.2.3, we can

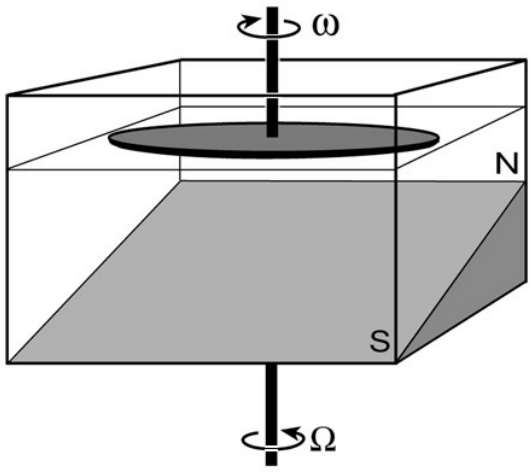

Figure 10.18: A tank with a false sloping bottom is filled with water so that the water depth varies between about 5 cm at the shallow end and 15 cm at the deep end. The slope of the bottom represents the spherical "beta-effect": the shallow end of the tank corresponds to high latitudes. (The labels N/S correspond to $\Omega > 0$, appropriate to the northern hemisphere). A disc is rotated very slowly at the surface of the water in a clockwise sense — a rate of 1 rpm works well. To minimize irregularities at the surface, the disc can be submerged so that its upper surface is a millimeter or so underneath the surface. The whole apparatus is then rotated in an anticlockwise sense on a turntable at a speed of $\Omega = 10$ rpm. It is left to settle down for 20 minutes or so. Holes bored in the rotating disc can be used to inject dye and visualize the circulation beneath, as was done in Fig.10.19.

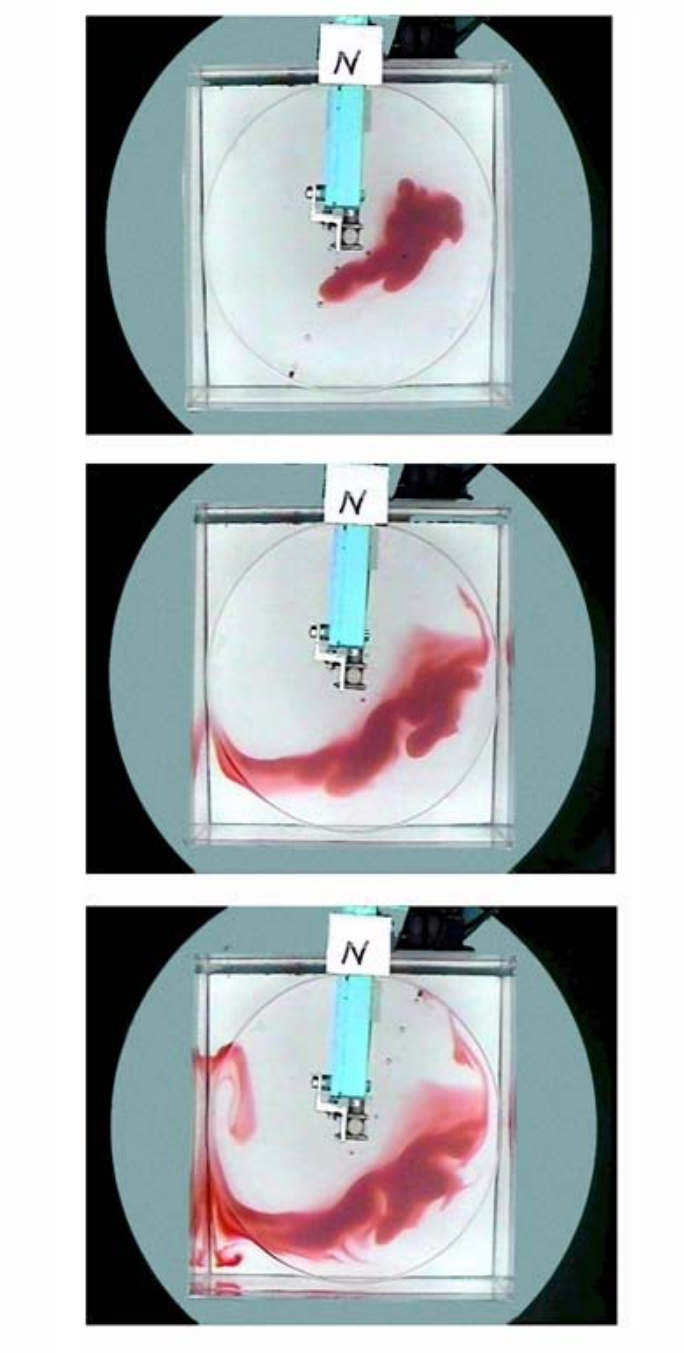

Figure 10.19: A time sequence (every 7 min) showing the evolution of red dye injected through a hole in the rotating disc. The label 'N' marks the shallow end of the tank. The plume of dye drifts "equatorward" in the 'Sverdrup' interior where Eq.(10.15) holds. In the bottom picture we see the dye being returned ploeward in a western boundary current, the laboratory model's analogue of the Gulf Stream or the Kuroshio. Equatorward flow is broad and gentle, poleward flow much swifter and confined to a western boundary current.

relate the strength of the north-south flow to the Ekman pumping from under the disc and the slope of the bottom, as follows (compare with Eq.(10.14)):

$$w_{Ek} = -\frac{Dd}{Dt} = -\frac{Dy}{Dt}\frac{\partial d}{dy} = -v\frac{\partial d}{dy} \tag{10.16}$$

where d is the depth of the water in the tank and where y here represents the upslope ("poleward") coordinate and v is the velocity in that direction. In our experiment, $w_{Ek} \simeq 5 \times 10^{-5}\,\mathrm{m\,s^{-1}}$ (as estimated for our Ekman experiment, GFD Lab XII above) and the bottom has a slope $\frac{\partial d}{dy} = -0.2$. Thus v should reach speeds of 2.5×10^{-4} $\mathrm{m\,s^{-1}}$ or 15 cm in 10 minutes or so directed equatorward (toward the deep end). This is broadly in accord with observed flow speeds.

The above relation cannot hold, however, over the whole domain because it implies that the flow is southward everywhere, draining fluid from the northern end of the tank. As can be seen in Fig.10.19, the water returns in a poleward flowing western boundary current, just as sketched in Fig.10.12.

10.3 The depth-integrated circulation: Sverdrup theory

One might wonder about the relevance of the homogeneous model of ocean circulation discussed above to the real ocean. The ocean is not homogeneous and it circulates in basins with complicated geometry — it is far from the homogeneous spherical shell of fluid sketched in Fig.10.15. And yet, as we will now see, the depth-integrated circulation of the ocean is indeed governed by essentially the same dynamics as a homogeneous fluid in a shallow spherical shell.

We begin by, just as in Section 10.2.1, eliminating (by cross-differentiation) the pressure gradient terms between the horizontal momentum balances, Eq.(10.3), to obtain, using continuity, Eq.(6.11):

$$\beta v = f\frac{\partial w}{\partial z} + \frac{1}{\rho_{ref}}\frac{\partial}{\partial z}\left(\frac{\partial \tau_y}{\partial x} - \frac{\partial \tau_x}{\partial y}\right)$$

which is Eq.(10.12) modified by wind-stress curl terms. Now, integrating up from the bottom of the ocean at $z = -D$ (where we imagine $w = 0$ and $\boldsymbol{\tau} = 0$) to the very top, where w is again zero but $\boldsymbol{\tau} = \boldsymbol{\tau}_{wind}$, we obtain:

$$\beta V = \frac{1}{\rho_{ref}} \left(\frac{\partial \tau_{wind_y}}{\partial x} - \frac{\partial \tau_{wind_x}}{\partial y} \right) = \frac{1}{\rho_{ref}} \widehat{\mathbf{z}} \cdot \nabla \times \boldsymbol{\tau}_{wind} \tag{10.17}$$

where

$$V = \int_{-D}^{0} v \, dz \tag{10.18}$$

is the depth integrated meridional transport. Eq.(10.17) is the result we seek — it is known as the 'Sverdrup relation'[6] and relates the vertically-integrated meridional flow to the curl of the wind stress. The key assumption that must be satisfied for its validity — in addition to $R_o << 1$ — is that flow in the deep ocean must be sufficiently weak (well supported by observation) so that both frictional stress on the ocean bottom and vertical motion are negligibly small.

Note the close connection between Eq.(10.17) and Eq.(10.15), (see Q3 at the end of the chapter, for a detailed look), when we realize that $hv = V$ is the transport and fw_{ek} is (if f were constant) the wind-curl divided by ρ_{ref} (cf. Eq.(10.7)). Thus, despite the apparent restrictions in the assumptions made in deriving Eq.(10.15), it turns out to have wide applicability. Moreover, when combined with the preference for western, as opposed to eastern, boundary currents, it gives us deep physical insights in to the mechanism underlying the wind-driven circulation.

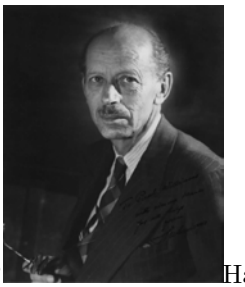

[6] Harald Ulrik Sverdrup (1888-1957), a Norwegian who began his career studying meteorology with Vilhelm Bjerknes in Oslo, was appointed director of Scripps Oceanographic Institution in 1936. His 1947 paper "Wind-driven currents in a baroclinic ocean", which showed the link between meridional currents and the curl of the wind stress, began the modern era of dynamical oceanography and initiated large-scale modeling of ocean circulation.

10.3.1 Rationalization of position, sense of circulation and volume transport of ocean gyres

The Sverdrup relation, Eq.(10.17), is one of the cornerstones of dynamical oceanography. We can use it to derive a simple expression for the transport of ocean gyres as follows. The depth integrated flow must be horizontally non-divergent and so we can introduce a streamfunction, Ψ, to map it out, [just as a streamfunction was used to represent the geostrophic flow in Section 7.1] where

$$U = -\frac{\partial \Psi}{\partial y};\ V = \frac{\partial \Psi}{\partial x}. \tag{10.19}$$

Combining Eqs.(10.17) and (10.19) and integrating westwards from the eastern boundary where we set $\Psi = 0$ (no transport through the eastern boundary[7]) we obtain:

$$\Psi(x,y) = \frac{1}{\rho_{ref}\beta} \int_{\text{eastern bdy}}^{x} \widehat{\mathbf{z}} \cdot \nabla \times \boldsymbol{\tau}_{wind}\, dx \tag{10.20}$$

This simple formula is remarkably successful — it predicts the sense of circulation and volume transport of all the major ocean gyres, rationalizing the patterns of ocean currents shown in Figs.9.14, 9.15 and 9.16 in terms of the pattern of imposed winds. Note, in particular, that Eq.(10.17) tells us that $V = 0$ along the lines of zero wind-stress curl, the thick black lines in Fig.10.11. Where $\widehat{\mathbf{z}}.\nabla \times \boldsymbol{\tau}_{wind} < 0$, $V < 0$ and *visa-versa*, allowing us to define subpolar and subtropical gyres etc and rationalizing the pattern of zonal jets observed in the tropical oceans, as sketched in the schematic diagram in Fig.10.20.

Fig.10.21 shows Ψ in the Pacific sector and should be compared with Fig.10.20. The curl of the annual-mean surface stress shown in Fig.10.2 was computed and integrated westwards from the eastern boundary to yield

[7]Since $U = 0$ at the eastern boundary, Eq.(10.19) tells us that Ψ is a constant there. Eq.(10.19) allows us to add any arbitrary constant to Ψ, so we are free to set $\Psi = 0$ at the boundary. Note, however, that we cannot simultaneously satisfy a vanishing normal flow condition through the western *and* eastern boundary using Eq.(10.17) because it involves only one derivative in x. As discussed in Section 11.3.3, dissipative processes must be invoked at the western boundary to obtain a complete solution. In Fig.10.21, the western boundary is sketched in as a feature required by mass continuity.

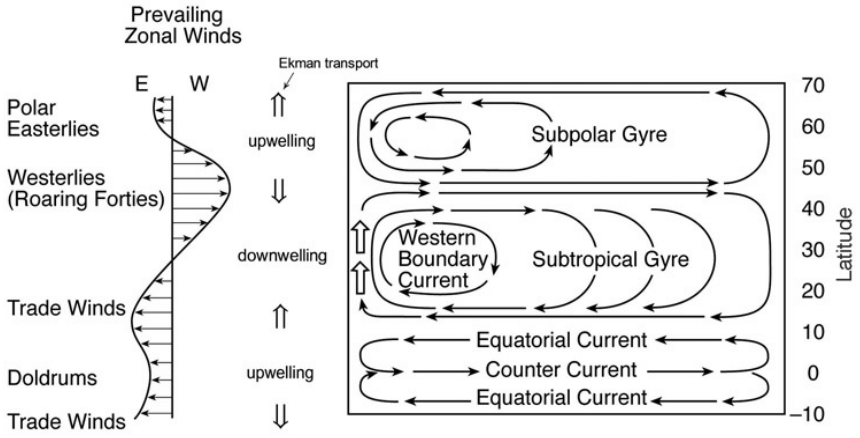

Figure 10.20: Schematic diagram showing the classification of ocean gyres and major ocean current systems and their relation to the prevailing zonal winds. The pattern of Ekman transport and regions of upwelling and downwelling are also marked.

Ψ from Eq.(10.20) as a function of horizontal position. The units are in $10^6\,\mathrm{m}^3\,\mathrm{s}^{-1}$: it is convenient to use 1 million cubic meters per second as a unit of volume transport which is known as the 'Sverdrup' (or Sv, after Harald Sverdrup). To put things in perspective, the flow of the Amazon river as it runs in to the sea is about 0.2 Sv: thus, transport of the subtropical gyre of the north Pacific is about 50 Sv or 250 times that of the Amazon, the biggest river on Earth!

One interesting rationalization provided by Sverdrup theory is that it accounts for the countercurrents (marked Equatorial Counter Current (ECC) in Fig.9.13) observed in the tropical oceans discussed in Chapter 9: i.e. currents that flow in a direction *opposite* to the prevailing winds. As can be seen in Fig.10.20 and 10.21, Sverdrup balance implies meridional flow away from the Doldrums in the interior with a return flow in a western boundary current. Convergence of these boundary currents drives an eastward flow just north of the equator, even though the winds are blowing toward the west here. This is just as observed in surface drifter data — see Fig.9.14 and the zonal-average surface currents across the Pacific plotted in the right-most panel in Fig.10.21.

The transport of the western boundary current must be equal and oppo-

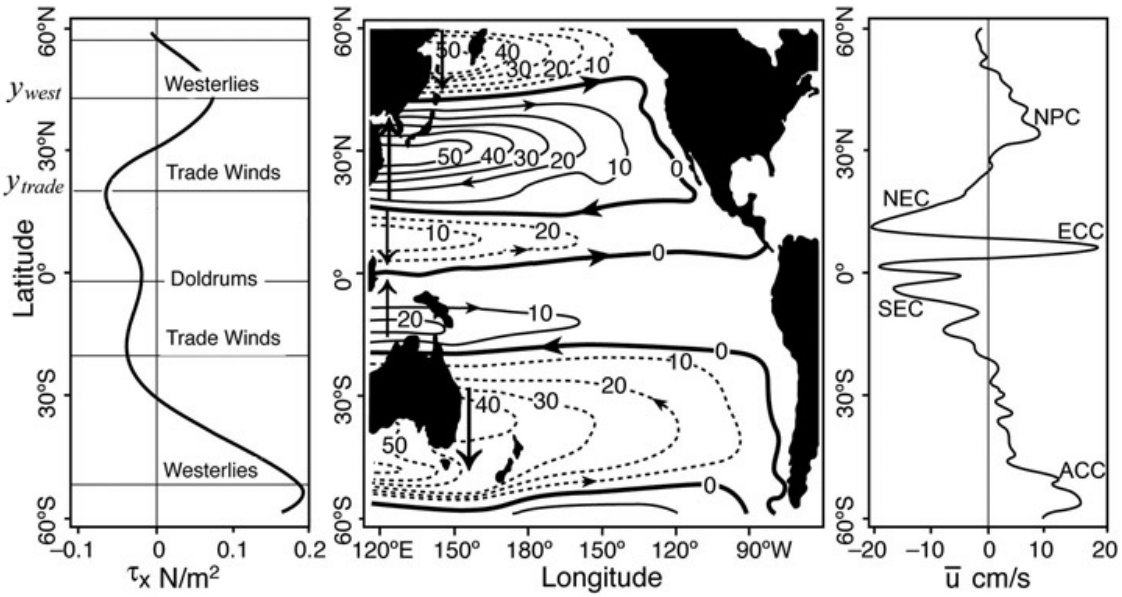

Figure 10.21: (left) The zonal-average of the zonal wind-stress over the Pacific ocean. (middle) The Sverdrup transport streamfunction (in $Sv = 10^6\,\mathrm{m}^3\,\mathrm{s}^{-1}$) obtained by evaluation of Eq.(10.20) using climatological wind-stresses, Fig.10.2. Note that no account has been made of islands — we have just integrated right through them. The transport of the western boundary currents (marked by the $N \leftrightarrow S$ arrows) can be read off from Ψ_{west_bdy}. (right) The zonal-average zonal current over the Pacific obtained from surface drifter data shown in Fig.9.14. Key features corresponding to Fig.9.13 are indicated.

site to that in the interior. The total interior transport is

$$\text{Int. Trans.} = \int_{\text{eastern bdy}}^{\text{western bdy}} V dx = \frac{1}{\rho_{ref}\beta} \int_{\text{eastern bdy}}^{\text{western bdy}} \widehat{\mathbf{z}} \cdot \nabla \times \boldsymbol{\tau}_{wind}\, dx = \Psi_{west\_bdy}, \tag{10.21}$$

and so the balancing boundary current transport, Ψ_{west_bdy}, can be read off Fig.10.21 — it is the value of Ψ at the western margin of the Pacific. However, it is instructive to obtain an explicit expression for the transport as follows. Let us assume that the wind-stress only has an east-west component (a useful approximation to reality, cf. Fig.10.2) so $\boldsymbol{\tau}_{wind} = (\tau_{wind_x}, 0)$ with $\tau_{wind_x} = -\tau_x \cos\left(\frac{\pi(y-y_{trade})}{L_y}\right)$ where $L_y = y_{west} - y_{trade}$ is a measure of the meridional scale over which the zonal wind changes from the westerly wind belt to the trades, as marked in Fig.10.21 (left most panel). Then, since $\widehat{\mathbf{z}} \cdot \nabla \times \boldsymbol{\tau}_{wind} = -\frac{\partial \tau_{wind_x}}{\partial y}$, Eq.(10.21) yields:

$$\text{Transport} = \frac{\pi\tau_x}{\rho_{ref}\beta}\frac{L_x}{L_y}\sin\left(\frac{\pi\,(y-y_{trade})}{L_y}\right)$$

where L_x is the east-west extent of the basin, assumed constant. Inserting numbers in to the above expression typical of the Pacific — $\tau_x = 0.1\,\mathrm{N\,m^{-2}}$, $\beta = 1.98\times10^{-11}\,\mathrm{m^{-1}\,s^{-1}}$, $L_y = 3000\,\mathrm{km}$; $L_x = 8000\,\mathrm{km}$ — we find a maximum transport of the subtropical gyre of 44Sv, roughly in accord with the detailed calculation given in Fig.10.21. The transport of the subtropical gyre of the Atlantic ocean is somewhat smaller, about 30Sv, largely on account of the much reduced east-west scale of the basin.

The interior Sverdrup transport of the gyre is thus returned meridionally in a narrow western boundary currents as marked in Fig.10.21 in the Pacific. In the Atlantic, it is clear from Fig.10.13 that the horizontal extent of the Gulf Stream is about 100 km. The hydrographic section of Fig.9.21(top) shows that the vertical extent of the region of strong lateral temperature gradients in the Gulf Stream is about 1 km. If a current of these dimensions is to have a transport of 30Sv then it must have a mean speed of some 30 $\mathrm{cm\,s^{-1}}$, roughly in accord with, but somewhat smaller than, direct measurement[8].

[8] The discrepancy is due to the fact that the transport of the Gulf Stream can considerably exceed the prediction based on Sverdrup theory because a portion of the fluid that flows in it recirculates in closed loops that do not extend far into the interior of the ocean.

Before going on, it should be mentioned that there is one major current system in Fig.9.13 which cannot be addressed in the context of Sverdrup theory — the Antarctic Circumpolar Current. The ACC is not in Sverdrup balance because there are no meridional barriers that allow water to be 'propped up' between them, hence supporting a zonal pressure gradient and meridional motion. Dynamically, the ACC is thought to have much in common with the atmospheric jet stream discussed in Chapter 8; eddy processes are central to its dynamics.

10.4 Effects of stratification and topography

Our analysis of the wind-driven circulation in Section 10.2 assumed the ocean to have constant density, whereas (see, e.g. Fig.9.7) the density of the ocean varies horizontally and with depth. In fact, the variation of density with depth helps us out of a conceptual difficulty with our physical interpretation in terms of the Taylor-Proudman theorem on the sphere presented in Section 10.2.3. We described how the Taylor columns of fluid must lengthen in the subtropical gyres, in order to accommodate Ekman pumping from above; where there is no Ekman pumping, they must maintain constant length. But the bottom of the ocean is far from flat. In the Atlantic Ocean, for example, there is a mid-ocean ridge that runs almost the whole length of the ocean rising about 2 km above the ocean bottom (see Fig.9.1). If the ocean were really homogeneous, water columns simply could not cross this ridge: there would be an enormous, elongated, stagnant "Taylor column" above it. And yet we have seen that homogeneous theory accounts qualitatively for the observed circulation, including the observation that, for example, the Atlantic subtropical gyre does indeed involve water flowing over the ridge. How does this happen?

In most regions the mean circulation, in fact, does not extend all the way to the bottom because, as discussed in Section 9.3.2, the interior stratification of the ocean largely cancels out surface pressure gradients. The thermal wind relation tells us that there can be no vertical shear in the flow of a homogeneous fluid since there are no horizontal density gradients. In the presence of density gradients the constraint of vertical coherence is weakened. Consider Fig.10.22. We suppose for simplicity that the ocean has two layers of different density ρ_1, ρ_2 (with $\rho_1 > \rho_2$, of course). The density difference produces a stable interface (somewhat like an atmospheric inversion described in Section

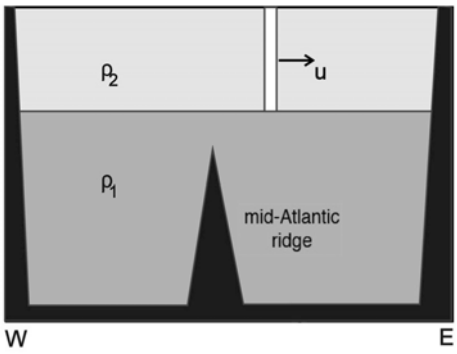

Figure 10.22: Upper layer Taylor column in a two layer idealization of the ocean moving over topography, such as the mid-Atlantic ridge confined to the lower layer.

4.4) which effectively decouples the two layers. Thus, Taylor columns in the upper layer, driven by Ekman pumping/suction from the surface, "feel" the interface rather than the ocean bottom. As long as the interface is above the topography, they will be uninfluenced by its presence. Thus, the density stratification "buffers" the flow from control by bottom topography. If we look at the density stratification in the real ocean (Fig.9.7), we see that most of the density stratification is found in the main thermocline, within a few hundred meters of the surface. Thus, the mean wind-driven circulation is largely confined to these upper layers.

10.4.1 Taylor-Proudman in a layered ocean

If we suppose that the ocean is made up of many layers of fluid with slightly differing densities, $\Delta\rho = \rho_1 - \rho_2$ etc, then we can imagine miniature 'Taylor Columns' within each homogeneous layer — and because each layer is homogeneous, T-P applies. Let's suppose that each Taylor column has a length d, measured parallel to the axis of rotation within each layer, as sketched in Fig.10.23. An interior column will try and maintain its length. Thus d is constant, as will be the quantity

$$\frac{2\Omega}{d} = \text{constant}.$$

which, using Eq.(10.13), can be written:

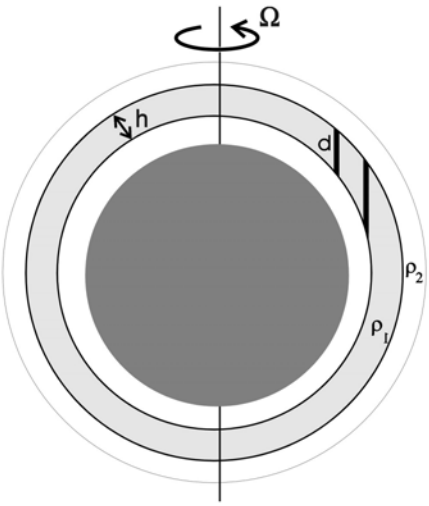

Figure 10.23: Miniature T-P columns in a layered fluid — the layers increase in density going downwards with $\rho_1 > \rho_2$.

$$\frac{f}{h} = \text{constant} \tag{10.22}$$

where f is the Coriolis parameter, Eq.(6.42), and h is the thickness of the layer in the direction of gravity measured in the vertical, as sketched in Fig.10.23.

If we focus on one particular layer then, away from the direct influence of Ekman pumping, $\frac{f}{h}$ will be conserved following that column of fluid around the ocean. What do the $\frac{f}{h}$ contours look like in the ocean? Some are plotted in Fig.10.24 for chosen density surfaces in the Pacific. In fact what is actually plotted is $\left(-\frac{f}{\rho_{ref}}\frac{\partial \sigma}{\partial z}\right)$, a 'continuous' version of $\frac{f}{h}$,[9] where σ is the potential density. On the $\sigma = 26.5$ surface in the North Pacific, for example, which is everywhere rather shallow (see Fig.9.8) the $\frac{f}{h}$ contours sweep around

[9] If h is the thickness of the layer across which the density changes by $\Delta\sigma$, then multiplying $\frac{f}{h}$ by $\frac{\Delta\sigma}{\rho_{ref}}$ we arrive at:

$$\frac{f}{h} \times \frac{\Delta\sigma}{\rho_{ref}} \longrightarrow \frac{f}{\rho_{ref}}\frac{\partial \sigma}{\partial z}$$

as h and $\Delta\sigma$ become small.

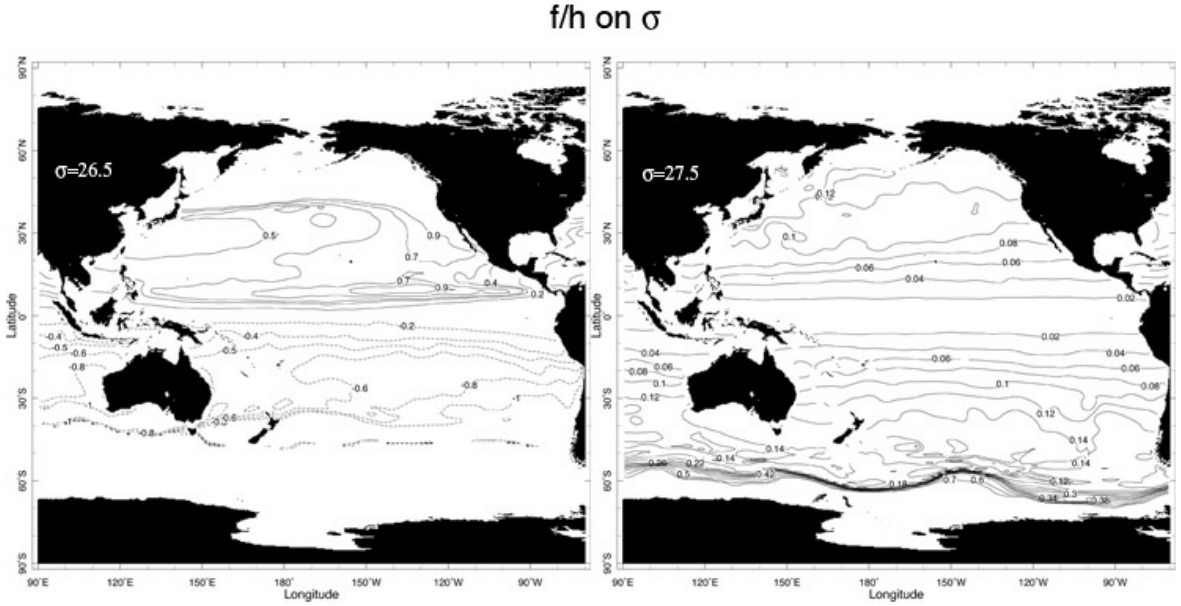

Figure 10.24: The quantity $\left(-\frac{f}{\rho_{ref}}\frac{\partial\sigma}{\partial z}\right)$ where σ is the potential density on a shallow density surface in the Pacific (left; $\sigma = 26.5$; the depth of this surface is plotted in Fig.9.8) and on a deeper density surface (right; $\sigma = 27.5$). Note that $\frac{\partial\sigma}{\partial z}<0$ because the ocean is stably stratified and so $\left(-\frac{f}{\rho_{ref}}\frac{\partial\sigma}{\partial z}\right)$ is positive in the Northern Hemisphere and negative in the Southern Hemisphere.

and turn back on themselves. Variations in h dominate over f allowing the strong circulatory flow of the gyre to persist within the thermocline without violation of Taylor-Proudman. On the $\sigma = 27.5$ surface, much deeper in the water column (see Fig.9.7), $\frac{f}{h}$ contours are more zonal and they intersect the coast. On these deeper surfaces, variations in f are much more important than variations in h. Since interior fluid columns conserve their $\frac{f}{h}$, there can be little flow deep down because the columns would run in to the coast. So the deep ocean interior is, in the mean, largely quiescent. However, as we shall see in Section 11.3 and 11.4, a weak abyssal circulation does exist fed by deep western boundary currents driven by convective sources at the poles. This is particularly true in the Atlantic (see, e.g., Fig.11.24).

10.5 Baroclinic instability in the ocean

In our discussion of the general circulation of the ocean in Chapter 9 it was emphasized that the mean circulation emerges only after long time averages. Instantaneously the flow is highly turbulent — see, e.g., Figs.9.19 and 9.22 and the numerical simulation shown in Fig.9.24. The sloping isopycnals evident in Fig.9.7 suggest that there is available potential energy (APE) in the ocean's thermocline. Indeed, following the analysis of Section 8.3.2, the ratio of APE to kinetic energy in the flow is, from Eq.(8.11), of order $\left(\frac{L}{L_\rho}\right)^2$. In the ocean the deformation radius, Eq.(7.23), has a value of $L_\rho = \frac{NH}{f} \simeq \frac{5\times10^{-3}\,\mathrm{s}^{-1}\times10^{3}\,\mathrm{m}}{10^{-4}\,\mathrm{s}^{-1}} = 50\,\mathrm{km}$ and so $\left(\frac{L}{L_\rho}\right)^2 \sim \left(\frac{1000\,\mathrm{km}}{50\,\mathrm{km}}\right)^2 = 400$ assuming that the mean flow changes over scales of 1000 km. Thus the potential energy stored up in the sloping density surfaces of the main thermocline represents a vast reservoir available to power the motion. This energy is tapped by baroclinic instability which fills the ocean with small-scale energetic eddies that often mask the mean flow. We can estimate expected eddy length scales and time scales using the arguments developed in Section 8.2.2 — see Eqs:(8.3) and (8.4). A deformation radius of 50 km yields eddy length scales of order 100 km. Growth rates are $\mathcal{T}_{eddy} \sim \frac{L_\rho}{U} = \frac{50\,\mathrm{km}}{10\,\mathrm{cm\,s}^{-1}} = 5\times10^5\,\mathrm{s}$, a week or so, significantly slower than that of atmospheric weather patterns. Eddy lifetimes in the ocean are considerably longer than those of their atmospheric counterparts; weeks and months rather than the few days of a typical weather system.

The mechanism by which APE is built up in the ocean is very differ-

ent from the atmosphere and, as we now describe, involves the collusion of mechanical (wind) and thermodynamic processes. In our discussion of the atmospheric general circulation in Section 8.3, we described how the net radiative imbalance led to warming in the tropics, cooling over the pole and hence the equator-to-pole tilt of θ surfaces and a store of available potential energy which can power the eddy field. In contrast, horizontal density gradients in the interior of the ocean and their associated store of APE are produced mechanically, by the same processes that drive the wind-driven currents, as illustrated in Fig.10.25. In the anticyclonic gyre, on the equatorward flank of the Gulf Stream, for example, Ekman pumping depresses isopycnals and isotherms by pumping light, warm water downward; poleward of the Gulf Stream, where the curl of the wind stress is cyclonic and there is a cyclonic gyre, Ekman suction lifts up the isopycnals and isotherms, as we saw in Fig.10.11. Thus, a horizontal density and temperature contrast is established across the current. In middle latitudes, then, the oceans have a thermal structure that is somewhat similar to that of the atmosphere, albeit maintained by a very different mechanism. In particular, the isopycnals slope poleward/upward — as sketched in Fig.10.25 — just as do θ surfaces in the atmosphere. Along with horizontal density gradients there is a reservoir of available potential energy which, through the agency of baroclinic instability, can be released into kinetic energy in the form of eddies, just as in GFD Lab XI[10]. Thus, oceanic eddies are analogs of midlatitude atmospheric eddies and have many similar properties. It is less clear, however, just how important oceanic eddies are in the "big picture" of the ocean circulation. They are certainly less crucial to effecting poleward heat transport than their atmospheric counterparts. This (as discussed in Chapter 11) is because the wind-driven and thermohaline circulations are quite capable of efficient poleward heat transport even in the absence of eddies. This contrasts with the atmosphere where, in middle latitudes, the zonal flow that would exist in the absence of eddies cannot transport heat, or anything else, in the N-S direction. In this context, the crucial difference between ocean and atmosphere is the E-W confinement of the oceans by continents, permitting western boundary currents and meridional transport. Note, however, that the ACC is not blocked by coasts and the mean flow is west-east: this is one place in the ocean where

[10]This statement refers to the midlatitude eddies evident in the height variance maps, Fig.9.19(bottom). The near-equatorial eddies evident in the surface current variance maps, Fig.9.22(bottom) are produced by another mechanism.

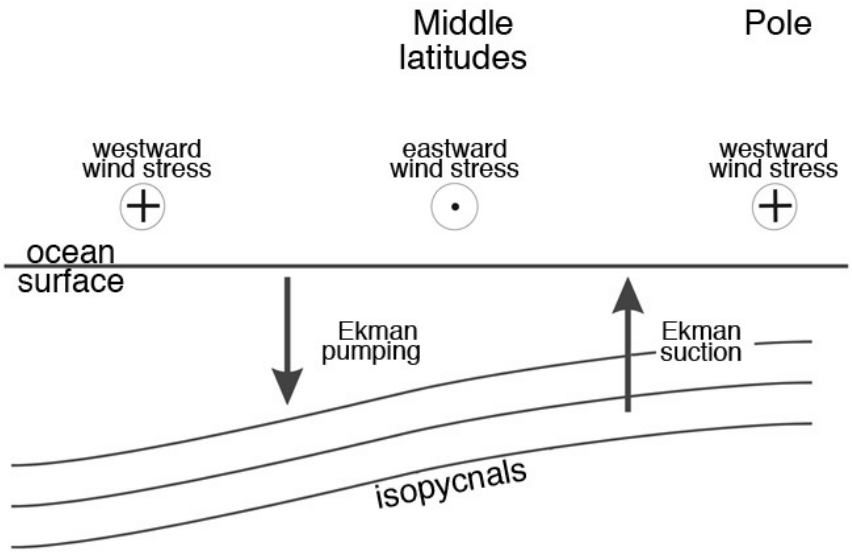

Figure 10.25: A schematic of the mechanism by which a large-scale sub-surface horizontal density gradient is maintained in the middle-latitude ocean. Ekman suction draws cold, dense fluid up to the surface in subpolar regions; Ekman pumping pushes warm, light fluid down in the subtropics. The resulting horizontal density gradient supports a thermal wind shear. Its baroclinic instability spawns an energetic eddy field which tends to flatten out the horizontal gradients.

eddies are known to play a central role in meridional property transport.

10.6 Further reading

Hartmann (1994) briefly reviews aspects of wind-driven ocean circulation theory and describes key observations. A (much) more detailed theoretical discussion can be found in Gill (1982), Rhines (1993), Pedlosky (1996) or Vallis (2006).

10.7 Problems

1. Consider the "Ekman layer" experiment, GFD Lab XII, Section 10.1.2. Assume the lid rotates cyclonically with respect to the turntable, as sketched in Fig.10.8. In addition to the Ekman layer at the base, there is a second layer at the lid. In this top Ekman layer, the effect of friction is to *drive* the flow, rather than to slow it down as at the base. Draw a schematic diagram showing the balance of forces in the top Ekman layer and use it to deduce the sense of the radial component of the flow. Contrast this with the bottom Ekman layer.

2. Fig.10.11 shows the pattern and magnitude of Ekman pumping acting on the ocean. Estimate how long it would take a particle of fluid to move a vertical distance of 1 km if it had a speed w_{Ek}. If properties are diffused vertically at a rate $k = 10^{-5}\,\mathrm{m^2\,s^{-1}}$ (typical of the main thermocline), compare this to the implied diffusive time-scale. Comment.

3. Use the results of Ekman theory to show that when one adds the meridional volume transport in the Ekman layer — given by Eq.(10.5) — to the meridional transport in the geostrophic interior — obtained from Eq.(10.12) — one obtains the Sverdrup transport, Eq.(10.17):

$$\frac{1}{\rho_{ref}}\mathbf{M}_{Ek_y} + \int_{-D}^{-\delta} v_g \; dz = \text{Sverdrup transport.}$$

4. Consider the Atlantic Ocean to be a rectangular basin, centered on 35°N, of longitudinal width $L_x = 5000\,\mathrm{km}$ and latitudinal width $L_y = 3000\,\mathrm{km}$.

   The ocean is subjected to a zonal wind stress of the form

$$\begin{aligned} \tau_x(y) &= -\tau_s \cos\left(\frac{\pi y}{L_y}\right) \; ; \\ \tau_y(y) &= 0 \; ; \end{aligned} \tag{10.23}$$

   where $\tau_s = 0.1\,\mathrm{N\,m^{-2}}$. Assume a constant value of $\beta = df/dy$ appropriate to 35°N, and that the ocean has uniform density $1000\,\mathrm{kg\ m^{-3}}$.

(a) From the Sverdrup relation, Eq.(10.17), determine the magnitude and spatial distribution of the depth-integrated meridional flow velocity in the interior of the ocean.

(b) Using the depth-integrated continuity equation, and assuming no flow at the eastern boundary of the ocean, determine the magnitude and spatial distribution of the depth-integrated zonal flow in the interior.

(c) If the return flow at the western boundary is confined to a width of 100 km, determine the depth-integrated flow in this boundary current.

(d) If the flow is confined to the top 500 m of the ocean (and is uniform with depth in this layer), determine the northward components of flow velocity in the interior, and in the western boundary current.

(e) Compute and sketch the pattern of Ekman pumping, Eq.(10.7), implied by the idealized wind pattern, Eq.(10.23).

5. From your answer to Question 4, determine the net volume flux at 35°N (the volume of water crossing this latitude in units of Sverdrups: Sv $= 10^6\,\mathrm{m}^3\,\mathrm{s}^{-1}$).

(a) for the entire ocean excluding the western boundary current

(b) for the western boundary current only.

(c) Assume again that the flow is confined to the top 500 m of the ocean. Determine the volume of the top 500 m of the ocean and, by dividing this number by the volume flux you calculated in part a., come up with a time scale. Discuss what this time scale means.

(d) Assume now that the water in the western boundary current has a mean temperature of 20 °C, while the rest of the ocean has a mean temperature of 5 °C. Show that $\mathcal{H}_{ocean}$, the net flux of heat across 35°N, is

$$\mathcal{H}_{ocean} = \rho_{ref} c_p \mathcal{V}\, \Delta T\ ,$$

where $\mathcal{V}$ is the volume flux you calculated in part (c), and ΔT is the temperature difference between water in the ocean interior and in the western boundary current. Recall that Fig.5.6 shows that the Earth's energy balance requires a poleward heat flux of

around 5×10^{15}W. Calculate and discuss what contribution the Atlantic Ocean makes to this flux.

6. Describe how the design of the laboratory experiment sketched in Fig.10.18 captures the essential mechanism behind the wind-driven ocean circulation. By comparing Eq.(10.16) with Eq.(10.12), show that the slope of the bottom of the laboratory tank plays the role of the $\beta-$effect: i.e. bottom slope $\longleftrightarrow \frac{1}{\tan\varphi}\frac{h}{a}$ where h is the depth of the ocean and a is the radius of the earth.

7. Imagine that the Earth was spinning in the opposite direction to the present.

   (a) What would you expect the pattern of surface winds to look like, and why (read again Chapter 8)?

   (b) on what side (east or west) of the ocean basins would you expect to find boundary currents in the ocean, and why?

   If you live in the southern hemisphere perhaps you are not scratching your head.

8. Use Sverdrup theory and the idea that only western boundary currents are allowed, to sketch the pattern of ocean currents you would expect to observe in the basin sketched below in which there is an island. Assume a wind pattern of the form sketched in the diagram.

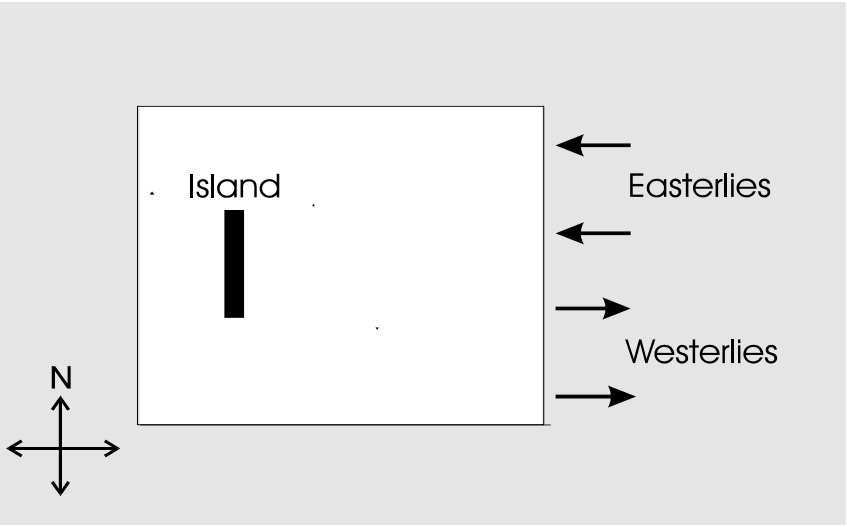

9. Fig.5.5 shows the observed net radiation at the top of the atmosphere as a function of latitude. Taking this as a starting point, describe the chain of dynamical processes that leads to the existence of anticyclonic gyres in the upper subtropical oceans. Be sure to discuss the key physical mechanisms and constraints involved in each step.